한국마린엔지니어링학회지 제36권 제5호, pp. 609~617, 2012. 7(ISSN 2234-8352 Online) / (ISSN 2234-7925 Print)
Journal of the Korean Society of Marine Engineering http://dx.doi.org/10.5916/jkosme.2012.36.5.609

Flow Characteristics of Polluted Air in a Rectangular Tunnel using PIV and CFD

Yong-Ho Lee†

(Received April 4, 2012; Revised April 24, 2012; Accepted July 11, 2012)

Abstract: The flow characteristics of polluted air are analysed by comparing the results obtained from PIV(Particle Image Velocimetry) experiment and CFD(Computational Fluid Dynamics) commercial code. In order to simulate the polluted air flow, the olive oil has been used as tracer particles with the kinematic viscosity of air, 1.51×10^{-5} m^2/s. The investigation has done in the range of Reynolds numbers of 870, 1730 and 2890 due to the inlet flow velocities of 0.3, 0.6, and 1.0 m/s, respectively. The average velocity and the pressure distributions are comparatively discussed with respect to the three different Reynolds numbers. The results show that the outlet flow rates at three different Reynolds numbers are equivalent of 165 to 167 percent of the inlet ones. The pressure drop occurs in the model closed at both end sides and the highest pressures at each Reynolds number are positioned at the top of the tunnel between the inlet and outlet.

Key words: Flow characteristics, Polluted air, Rectangular tunnel, PIV(Particle Image Velocimetry), CFD(Computational Fluid Dynamics)

1. Introdution

The tunnel is one of the important facilities of railroad and highway transportation, and also a throat of railroad and highway. With the development of transportation, plenty of tunnels are constructed and still under construction in the most parts of the world. It is required to be designed for terminal devices along the tunnel to control polluted air such as smoke or poisonous gas produced inside the tunnels. Extreme damages due to the polluted air in a long corridor or tunnel threaten the people's life. What is worse, the narrow and enclosed special construction inside the tunnel does not easily lead to the vehicles and personnels out a safer place.

A turbulent flow in a rectangular tunnel is an active area of research because of its wide practical applications to heat exchanger tube bundles, to smoke exhaust devices, and to cooling systems for nuclear power plants[1]. So there has been a considerable amount of theoretical and experimental works committed to the study of different aspects of laminar or turbulent flow structure in rectangular tunnels or tube bundles.

The analysis of turbulent flow phenomena in a rectangular tunnel has been studied by many investigators so far. Aiba et al[2]. observed a mean and turbulent intensity measurement in inline and staggered tube bundles using a two-component hot-wire anemometer when the pitch ratios were arranged from 1.2 to 1.6 and the Reynolds number was 30000. Kim et al[3]. performed flow visualization in rectangular ducts, in which the aspect ratios were 1/2 and 1/5. Bonhoff et al[4].

† Corresponding Author (Dept. of Mechanical-Automotive Engineering, Chonnam National University, Yeosu Campus, E-mail: toleeyongho@hotmail.com, Tel: 061-659-7280)

investigated experimentally and numerically the flow characteristics in a coolant square channel with 45 degree ribs.

The flow characteristics in various fluid dynamics models on different boundary conditions are analyzed by two typical tools: the PIV(Particle Image Velocimetry) data acquisition and the CFD(Computational Fluid Dynamics) analysis. PIV system provides instantaneous velocity fields over global domains and records the position over time of small tracer particles introduced into the flow to extract the local fluid velocity[5]. It is used to study the flow characteristics in a rectangular tunnel by providing instantaneous velocity vectors and mean vorticity fields[6, 7]. As for the reliable whole field measurement technique and lots of special implementations in the PIV system, the instantaneous velocity fields, pressure distributions, vorticity maps, turbulent intensity, and kinetic energy fields are provided [8, 5]. Although having a lot of advantages for the system, it is difficult to quantify the concentration variations of the polluted air by conducting a modeling experiment completely.

The CFD tools remain the most powerful method to predict the flow behavior, which has the strong points such as accuracy, convenience, and cost-saving. Therefore, the application of CFD has become widespread for various engineering problem solving. Nuri et al[9]. conducted an experimental and numerical study to investigate fire behaviors in a scaled version of an underground station. The general flow pattern and the back-layering in velocity measured experimentally in the station at different locations are shown to be well matched by the CFD simulations. Wu & Baker[10] and Hwang & Wargo[11] had compared the simulation results from smoke movement in longitudinally ventilated tunnels with the experimental data. Hwang and Edwards[12] carried out a study on the critical ventilation velocity in inclined tunnels. Francesco Colella, et al[13]. applied a transient multiscale approach to model ventilation flows and fires in a tunnel domain using CFD.

In this paper, air flow characteristics in a rectangular tunnel have been observed by using the ANSYS CFX code and the PIV data acquisition system. The experimental results of the flow characteristics about the velocity components alone in the rectangular tunnel model are compared with the CFD results by means of three different Reynolds numbers. The other main objectives are to analyze air flow characteristics regarding pressure distributions and kinetic energy fields in a rectangular tunnel closed at both end sides using CFD and to provide available information about better design of a tunnel ventilation system.

2. Experimental PIV Approach

In the PIV system, an optically transparent test section to visualize the flow motion should be made to observe tracer particles by using a light source for the data acquisition. **Figure 1** shows the experimental test section made by a transparent acrylic rectangular tunnel model. The length, height, and width of the tunnel model are 800mm, 80mm, and 80mm, respectively. The inlet is placed in the middle of the tunnel floor, while the outlet is located on the right side on the tunnel ceiling in the x direction. The longitudinal distance from the vertical centerline of the inlet to the outlet on the ceiling is specified as L = 60mm. The rectangular cross-sectional dimension of the inlet and the outlet is 30mm × 80mm.

The aspect ratio of this model, which is the ratio of the tunnel length of 800mm to the hydraulic diameter of 80mm, is 10. A scale model 100 times smaller is made and tested. These assumption might not be completely reasonable in some cases, but in order to discuss the flow characteristics in the

rectangular tunnel model the similarity is considered to be useful between the prototype and the model.

The olive oil particles made by an air compressor enters the rectangular tunnel through the plastic-pipe and then exits through the outlet on the ceiling.

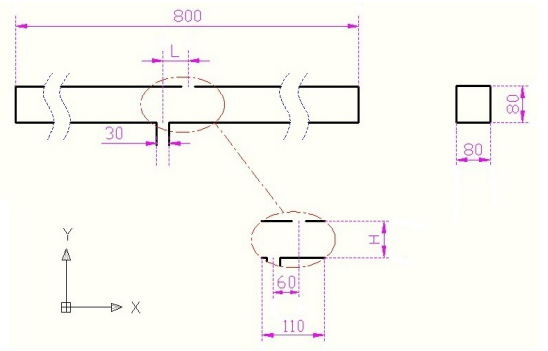

Figure 1: Test section in PIV experiment. (L = 60mm and H = 80mm)

A plastic trunk and a small axial fan is used to find a steady state at low velocity. Each image is captured by the CCD camera which is positioned at right angle to the light-sheet in the Dantec PIV 2000 system. The each image corresponds to two pictures taken at time T and T+△t as well. Then the pictures are transmitted into the PIV processor software Flow Manager. For reasons of experimental reproducibility, the raw vector/scalar map is archived and a new validated vector map is output by the software. Further analysis can produce streamlines, vorticity, kinetic energy, turbulent intensity by using the PIV system.

3. CFD Simulation

In order to investigate the velocity fields, the pressure distributions and the kinetic energy fields in the tunnel model, ANSYS CFX, which is a commercial CFD program, has been implemented for this paper. The tunnel modeling and the boundary conditions in the test section are the same as the those of the previous experiment[7] using PIV. The material properties of working fluid here are chosen as the ambient air.

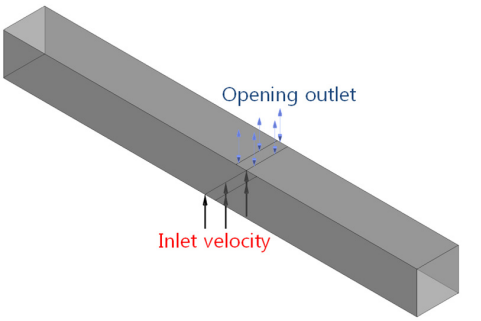

Figure 2: Boundary conditions for rectangular tunnel at L = 60 mm.

To create grids from the geometry for this study, the grid generation tool of ANSYS ICEM CFD was used. In order to formally reduce or remove the grid dependency of the boundary condition, around 300,000 quadrilateral grids are meshed in order to identify the flow characteristics for good grid quality in dealing with the dimensions of the domain in the tunnel model. Since the wall boundary condition is formally grid dependent, the grids as shown in **Figure 3** are also concentrated in the region near the tunnel walls to satisfy the wall conditions. No-slip boundary conditions are imposed on all sides of the wall inside the tunnel.

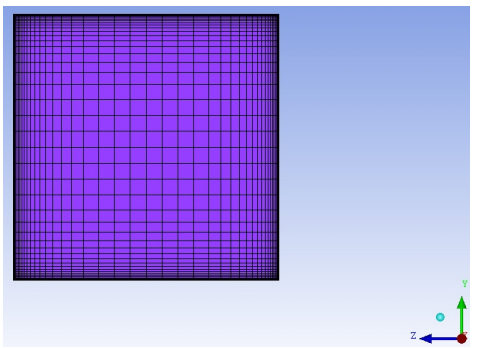

Figure 3: Computational mesh for near-wall boundary condition

The inlet flow velocities of 0.3 m/s, 0.6 m/s, 1.0 m/s under the same conditions conducted in the experimental approach. For simulating laminar and turbulent flows, the RNG k-ε model is used for predicting indoor airflows effectively in tunnel models[14]. These laminar and turbulence models have been proposed for good overall performance in occurring near separation points of the flow in the near-wall region. The CFD calculations for the 3-D simulation have been performed under steady-state conditions to evaluate the flow characteristics in the tunnel modeling. For convergence, RMS(root mean square) normalized values of the equation residuals is applied and the target residual value is 0.00001.

4. Results and Discussions

The experimental flow is an atomizing air from the atomizer in order to control and change the three different speeds in the experiment. The air flow characteristics in the tunnel have been researched at three different Reynolds numbers. To observe flow behavior related to velocity vectors experimentally, olive oil as tracer particles has been used with the kinematic viscosity of air, 1.51×10^{-5} m^2/s. Tracer particles are observed as a source of the polluted air in the experimental process. According to the variation of the Reynolds number, the average velocity vector field, pressure distributions, and kinetic energy are discussed by depicting the flow distributions throughout the domain in the paper.

4.1 The average velocity vector graph

In **Figures 4** to 6, the mean velocity vector fields using CFD and PIV are shown depending on the three different Reynolds numbers of 870, 1730, and 2890. In order to show the flow velocity fields at the inlet and outlet, a cross-sectional image of 110mm × 80mm area has been examined by using PIV and CFD as shown in **Figure 1**. The inlet (30mm × 80mm) is located at the middle of the floor in the x-z bottom plane, while the outlet is positioned on the ceiling to the right side of 60mm away from the centerline of the inlet position.

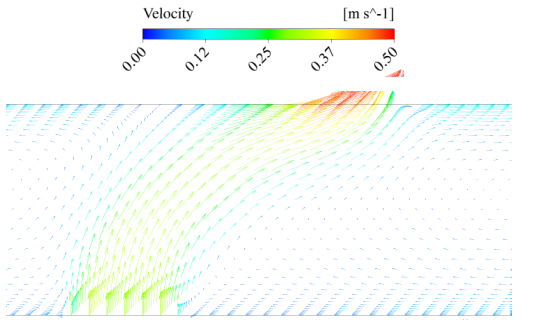

(a) Velocity vector field using CFD

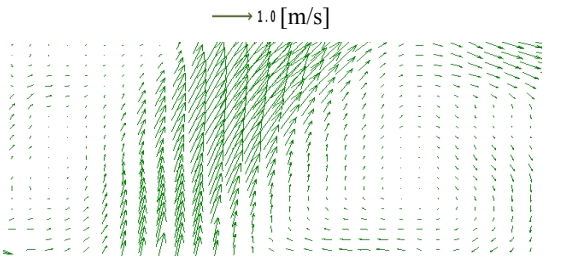

(b) Instantaneous velocity vector field using PIV

Figure 4: Velocity vector fields using CFD and PIV at Re=870

Figure 4 shows the velocity vector fields using CFD and PIV at the Reynolds number of 870. A large recirculation zone is found on both sides of the flow motion between the inlet and the outlet in the tunnel model. It is considered to be caused by a collision with the tunnel ceiling and the tunnel walls at a very low velocity. It implies that some air flow along the ceiling layer is exhausted into the outlet and the rest of air flow goes towards inside the tunnel again. It is also observed that the maximum value of mean velocity occurs in the inlet and outlet regions in **Figure 4**(a). The air flow velocity at the floor level of the tunnel is lower

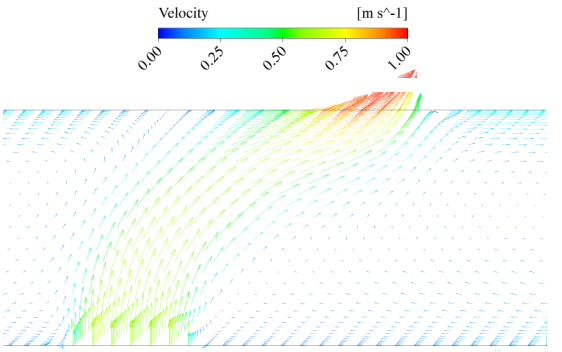

(a) Velocity vector field using CFD

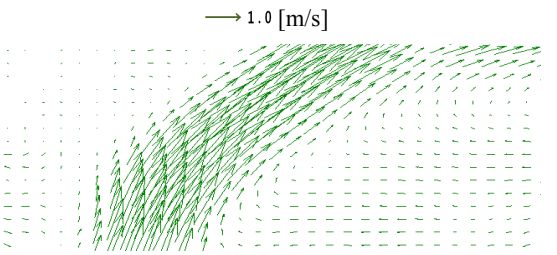

(b) Instantaneous velocity vector field using PIV

Figure 5: Velocity vector fields using CFD and PIV at Re=1730

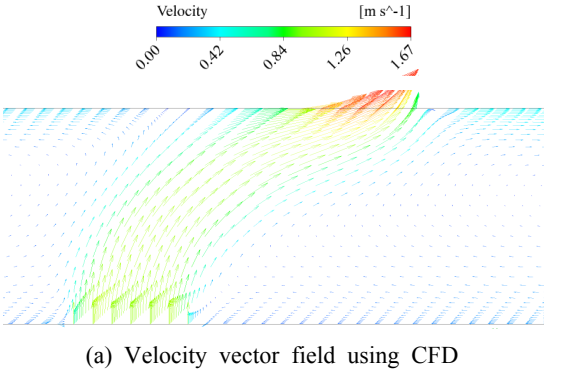

(a) Velocity vector field using CFD

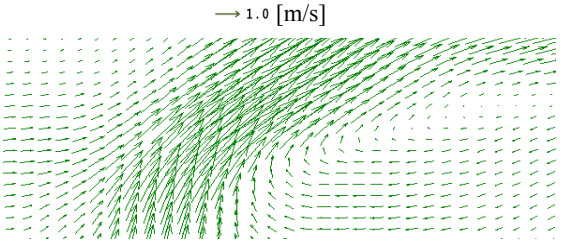

(b) Instantaneous velocity vector field using PIV

Figure 6: Velocity vector fields using CFD and PIV at Re=2890

than that at or near the inlet and outlet regions. It is helpful to make a decision with regard to the emission rates of polluted air and to make people escape from a danger zone toward the leeward direction. In **Figure 4**(a), the recirculation region is partially placed to the direction of the outlet compared to that region shown in PIV, in which the recirculation flow is produced just below the outlet position. It is considered that the experimental boundary conditions are a little incomplete. In addition, it is assumed that some problems are caused by heavy emissions produced by the atomizer in a very short time while doing the experiment and also in particular at a low Reynolds number of 870, the density difference between the air containing olive oil as trace particles in PIV and the ambient air alone in CFD approach has a little influence on the flow behavior. However, some similar trends between them are exhibited.

As the Reynolds number increases to 1730, as shown in **Figure 5**, the flow velocity of air near the top of tunnel is significantly higher than that of the bottom. Increasing the longitudinal air velocity makes more air flow circulate inside the tunnel model. The vortex which is found near the middle layer of the tunnel just below the outlet is more active.

As the Reynolds number increases up to 2890, as shown in **Figure 6**(b), some vortices are not shown completely here but the vortex intensity is a little higher at the upper part of the tunnel near the outlet region and also at other lower parts according to the PIV measurement. As the inlet flow velocity increases, the outlet velocity on the tunnel ceiling increases. Comparing with the Reynolds number of 1730, the case of the Reynolds number of 2890 belonged to the turbulent flow exerts a higher influence on exhausting the polluted air.

In CFD, the maximum velocities of air flow given at the outlet at each Reynolds number of 870, 1780, and 2890 are 0.496, 0.997, and 1.670 m/s, respectively. The values of incremental velocity change between the inlet and outlet at three Reynolds numbers are 0.196, 0.397 and 0.670. The outlet flow rates at three different Reynolds numbers are equivalent of 165 to 167 percent of the inlet ones. As the Reynolds number increases, the outlet flow velocity simultaneously increases. However, the change of the outlet flow rates is almost identical when compared with the inlet ones. It is considered to be a typical phenomenon caused by the effects of the pressure change inside the tunnel model. With the increase of Reynolds numbers, the flow behavior is more in disorder and the region of finite recirculation is subjected to the air velocities through the inlet flow.

4.2 Pressure distributions using CFD analysis

In order to get better visualization for pressure distributions, the vertical dimension has been enlarged in the x-y plane. **Figure 7** shows the pressure distribution using CFD analysis along with three different Reynolds numbers in the rectangular tunnel model which is closed at both end sides. The outlet is installed at 60 mm away on the ceiling in the x-z plane from the centerline of the inlet.

The pressure is generally low at the inlet, while it attains to the maximum value on the left side of the outlet in the ceiling zone. **Figure 7**(a) shows the pressure contours at Reynolds number of 870. Even though the pressure distributions are all over low, the pressure in the inlet region is a little lower than the other regions on the tunnel floor. In general the pressure distribution is horizontally stratified due to the low inlet velocity. The peak in the pressure distribution is located near the ventilated opening on the tunnel ceiling.

In **Figure 7**(b) the pressure variations are most noticeable in the vicinity of the outlet. As the Reynolds number increases to 1730, the higher pressure drop between the inlet and outlet occurs compared with the case of Reynolds number 870. Flow behavior inside the tunnel is primarily in the upward direction to exhaust the air to the outlet. In the region with no ventilation a little far away from the outlet, the pressure distributions are usually horizontal in most cases in the tunnel.

As shown in **Figure 7**(c), the range of the higher pressure on the ceiling grows bigger and wider due to the increasing Reynolds number. It is assumed that the inlet flow due to the high velocity impinges on the ceiling wall. On the other hand, the pressure on the tunnel floor is lower in most cases. The highest value of pressure distribution is shown on the left side of the outlet due to the highest inlet flow velocity. The pressure change between the inlet and outlet is also largest compared with those of two lower Reynolds numbers.

In the model closed at both end sides, the pressure drops occur because the inlet pressure is higher than the outlet. The pressure drops, $\Delta P_{tunnel} = P_{inlet} - P_{outlet}$, are caused by the pressure difference between the inlet and outlet inside the tunnel. In the case of three Reynolds number of 870, 1730, and 2890, the pressure drops are 0.035, 0.346, and 1.053 Pa, respectively. Even though pressure changes are small enough, in other words, the pressure drops are relatively increased in the model as the Reynolds number increases. The highest pressures at each Reynolds number are 0.148, 0.557, and 1.534 Pa, respectively, which are positioned at the top of the tunnel model on the left side of the outlet, or in the uppermost part between the inlet and outlet. The pressure distribution through the inlet and outlet can be investigated by the CFD analysis and be used for

better tunnel design to be properly taken into consideration.

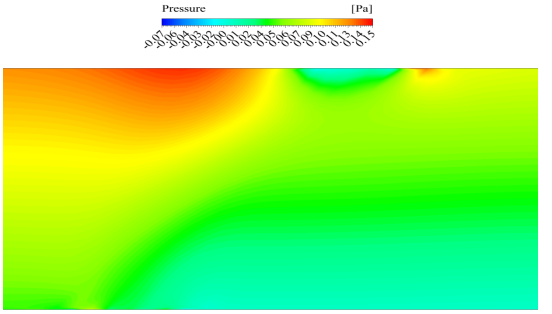

(a) pressure contours at Re = 870

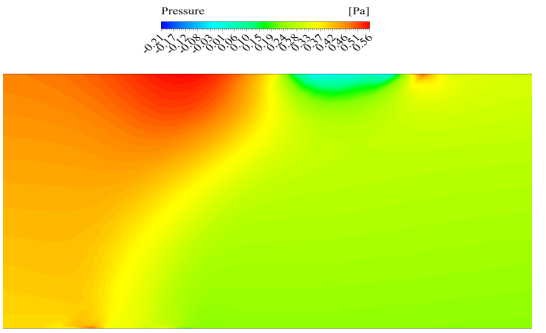

(b) pressure contours at Re = 1730

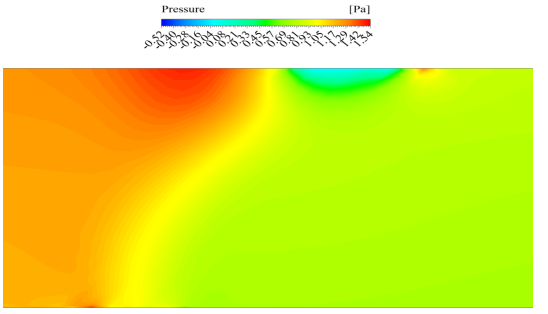

(c) pressure contours at Re = 2890

Figure 7: Predicted pressure distributions using CFD analysis along with different Reynolds numbers in the rectangular tunnel

4.3 Kinetic Energy Field

As shown in **Figure 8**, the highest kinetic energy is distributed near the outlet region at all Reynolds numbers here, in spite of having such a low energy of 0.1 to 0.15 m^2/s^2 (a unit mass is neglected) in all tunnel flow regimes. The bulk of considerable kinetic energy spreads widely in the vicinity of the outlet region. As the Reynolds number increases, the instantaneous kinetic energy obtained from the experimental data by PIV increases in disorder. However, the kinetic energy by CFD is regularly distributed, though the Reynolds number increases. The trend of kinetic energy distributions is almost similar along the track followed by the flow motion, although the amounts of laminar or

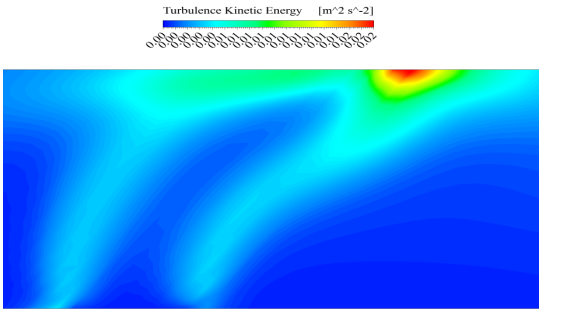

(a) kinetic energy contour at Re=870

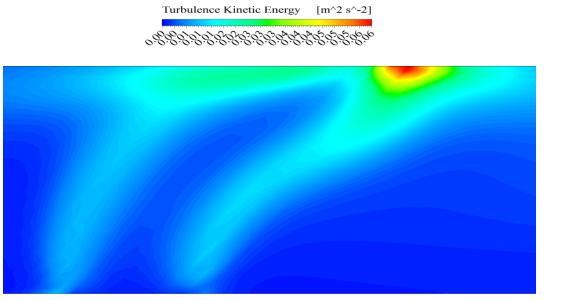

(b) kinetic energy contour at Re=1730

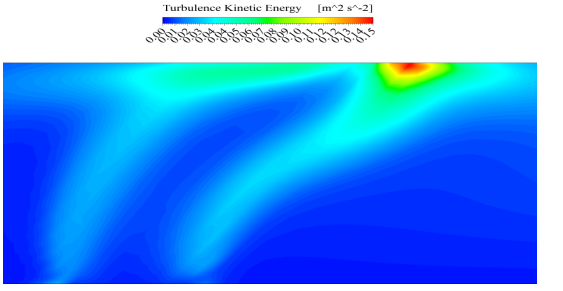

(c) kinetic energy contour at Re=2890

Figure 8: Kinetic energy plots for various Reynolds numbers by CFD

turbulence kinetic energy have a slight difference due to the three different Reynolds numbers. The kinetic energy is distributed, with tilted slightly to the right, along both sides of the path from the inlet to the outlet. With the increase of Reynolds numbers, the amount of kinetic energy generally has a rapid increase. The corresponding kinetic energy can be converted into a pressure change inside the tunnel. It is considered that the rectangular opening on the ceiling has an effect on the ventilation system in the tunnel. These results show that an appropriate ventilation or opening must be maintained to provide the evacuation way for people in danger.

5. Conclusions

In this work, an experimental and numerical study based on three different Reynolds numbers has analyzed by the velocity vector fields, the pressure distributions, and the laminar or turbulent kinetic energy in the rectangular tunnel model. The main findings of this study are:

(1) Even though the recirculation regions obtained from PIV system and CFD analysis do not have a complete agreement, the flow behaviors are considerably similar as a whole. The better way to make the polluted air exhaust out the tunnel model is given by considering the velocity vector field.

(2) The maximum velocities of air flow are shown at the outlet at each Reynolds number. The outlet flow rates at three different Reynolds numbers are equivalent of 165 to 167 percent of the inlet ones. As the Reynolds number increases, the outlet flow velocity simultaneously increases. However, the change of the outlet flow rates is almost identical when compared with that of the inlet ones. It is considered to be a typical phenomenon caused by the effects of the pressure change inside the tunnel model. With the increase of Reynolds numbers, the flow behavior is more in disorder and the region of finite recirculation is subjected to the air velocities through the inlet flow.

(3) The pressure drop occurs in the model because the inlet pressure is higher than the outlet. In the case of three Reynolds numbers of 870, 1730, and 2890, the pressure drops are 0.035, 0.346, and 1.053 Pa, respectively. The highest pressures at each Reynolds number are 0.148, 0.557, and 1.534 Pa, respectively, which are positioned at the top of the tunnel model on the left side of the outlet, or in the uppermost part between the inlet and outlet.

(4) The kinematic energy increases due to the pressure change in the tunnel, as the Reynolds number increases. It is considered that the outlet through the tunnel ceiling has a large effect on the ventilating system in the tunnel model.

(5) Moreover, various flow phenomena including flow velocity and pressure distributions, turbulence intensity, and vorticity can be analyzed by the comparison of PIV and CFD approaches for further study and can be available for better tunnel design.

References

[1] Juliss Brandies and Daniel J. Begmann "A numerical study of tunnel fires". Combustion Sci. and Tech, vol. 35 pp. 133-155, 1983.

[2] S. Aiba, H. Tsuchida and T. Ota, "Heat transfer around tubes in in-line tube banks", Bull. Journal of the Japan Society of Machanical Engineers, vol. 25, pp. 919-926, 1982.

[3] W.J. Kim and V.C. Patel, “Origin and decay of longitudinal vortices developing in a curved rectangular duct”. J. Fluids Eng. vol. 116, pp. 45-51, 1994.

[4] B. Bonhoff, S. Parneix et al. “Experimental and numerical study of developed flow and heat transfer in coolant channels with 45

degree ribs", Int. J. Heat Fluid Flow 20 pp. 311-319, 1999.

[5] Dantec Dynamics, FlowManger software and introduction to PIV: 2D PIV Installation and User's Guide, 2000.

[6] Sang-Kyoo Park, Hei-Cheon Yang, Yong-Ho Lee and Gong Chen, "PIV measurement of the flow field in Rectangular Tunnel," Journal of the Korean Society of Marine Engineering, vol. 32, no. 6, pp. 886-892, 2008.

[7] Yong-Ho Lee, "Experimental and CFD simulations of polluted air behavior in rectangular tunnels," Journal of the Korean Society of Marine Engineering, vol. 35, no. 5, pp. 608-615, 2011.

[8] M. Raffel, C. Willert and J. Kompenhans, Particle Image Velocimetry, A Practical Guide, Springer, pp. 88-123, 1998.

[9] Nuri Y, Muhammed I.B., Salih K, and Nureddin D, "Experimental and numerical simulation of fire in a scaled underground station," World Academy of Science, Engineering and Technology, vol 40, pp. 309-314, 2008.

[10] Wu, Y. and Baker, M.Z.A, "Control of smoke flow in tunnel fires using longitudinal ventilation systems - a study of the critical velocity", Fire Safety Journal, vol. 35, pp. 363-390, 2000.

[11] C.C. Hwang, JD. Wargo, "Experimental Study of thermally generated reverse stratified layers in a fire tunnel." Combust Flame, vol. 66, pp. 171-180, 1986.

[12] C.C. Hwang, J.C. Edwards, "The critical ventilation velocity in tunnel fires - a computer simulation," Fire Safety Journal, vol. 40, pp. 213-244, 2005.

[13] F. Colella, G. Rein, V. Verda, R. Borchiellini, "Multiscale modeling of transient flows from fire and ventilation in long tunnels", Journal of Computers & Fluids, vol. 51, pp. 16-29, 2011.

[14] V. Yakhot and S.A. Orszag, "Renormalization group analysis of turbulence", Journal of Scientific Computing, vol. 3, pp. 3-51, 1986.